İstanbul Med J 2026; 27(3): 245-51
**DOI:** 10.4274/imj.galenos.2026.52284

# Magnetic Resonance Imaging Texture Analysis for Predicting Chemoradiotherapy Response in Locally Advanced Rectal Cancer

Murat Özoğul[1], Kamil Canpolat[2], Eşref Başaran[3], Murat Baykara[4]

[1]University of Health Sciences Türkiye, İstanbul Training and Research Hospital, Clinic of Radiology, İstanbul, Türkiye
[2]Medicalpark İzmir Hospital, Clinic of Radiology, İzmir, Türkiye
[3]University of Health Sciences Türkiye, Sultan 2. Abdülhamid Han Training and Research Hospital, Clinic of Radiology, İstanbul, Türkiye
[4]University of Health Sciences Türkiye, Haydarpaşa Numune Training and Research Hospital, Clinic of Radiology, İstanbul, Türkiye

## ABSTRACT

**Introduction:** This study investigated the predictability of treatment response to neoadjuvant chemoradiotherapy (nCRT) using texture analysis derived from pre-treatment magnetic resonance imaging (MRI) in patients diagnosed with locally advanced rectal cancer (LARC).

**Methods:** A total of 47 patients (28 males and 19 females) diagnosed with LARC who received nCRT between 2018 and 2025 were retrospectively reviewed in the hospital archives. Texture analysis was performed on pretreatment MR images, specifically on T2-weighted images, apparent diffusion coefficient (ADC) maps, and contrast-enhanced T1-weighted images. For the assessment of treatment response, patients were classified according to the modified Ryan tumor regression grading system: those with Ryan grades 0 and 1 were assigned to the favorable response group, while those with Grades 2 and 3 were assigned to the poor response group. Statistical analysis was conducted using the Mann-Whitney U test, receiver operating characteristic curve analysis, and multivariable logistic regression.

**Results:** Statistically significant differences were detected between the responding and non-responding groups across 44 texture parameters in the three sequences. The multivariable logistic regression model was statistically significant ($p<0.001$). A combined predictive model, including the contrast of matrix from the ADC sequence and the contrast of matrix and energy of matrix from the contrast-enhanced T1-weighted sequence, explained 74.3% of the variance in treatment response and correctly classified 91.3% of the patients.

**Conclusion:** Texture analysis derived from pre-treatment magnetic MR imaging can predict the response to neoadjuvant therapy with high accuracy in patients with LARC. This non-invasive approach demonstrates considerable potential as a clinical tool to guide personalized treatment strategies, thereby facilitating the selection of optimal therapeutic regimens for patients who are unlikely to benefit from standard protocols.

**Keywords:** Rectal cancer, magnetic resonance imaging, texture analysis, radiomics, chemoradiotherapy

## Introduction

Colorectal cancer is the third most frequently diagnosed cancer worldwide, with rectal cancer accounting for approximately 40% of all cases. It ranks third in incidence among men, whereas among women, it is the second most common malignancy (1,2). The incidence of colorectal cancer is disproportionately higher in Western countries, a trend that has been consistently associated with lifestyle-related risk factors such as obesity, metabolic syndrome, and dietary patterns rich in red and processed meats but low in fiber (3).

In patients with suspected rectal cancer, magnetic resonance imaging (MRI) has emerged as the modality of choice for the diagnosis of rectal cancer because of its superior soft tissue contrast and multiplanar imaging capabilities. MRI allows accurate evaluation of tumor size, local extension, and circumferential resection margin involvement, as well as precise assessment of regional lymph nodes and potential metastatic disease. Furthermore, MRI is invaluable for monitoring treatment response after neoadjuvant therapy and detecting local recurrence following surgical resection, thereby playing a central role in guiding treatment strategies and long-term patient management (4-6).

**Address for Correspondence:** Murat Özoğul, MD, University of Health Sciences Türkiye, İstanbul Training and Research Hospital, Clinic of Radiology, İstanbul, Türkiye
**E-mail:** muratozogl@gmail.com **ORCID ID:** orcid.org/0000-0001-5825-911X
**Cite this article as:** Özoğul M, Canpolat K, Başaran E, Baykara M. Magnetic resonance imaging texture analysis for predicting chemoradiotherapy response in locally advanced rectal cancer. İstanbul Med J. 2026; 27(3): 245-51

**Received:** 22.04.2026
**Accepted:** 06.07.2026
**Publication Date:** 03.08.2026

The standard treatment protocol for locally advanced rectal cancer (LARC) consists of neoadjuvant chemoradiotherapy (nCRT) followed by total mesorectal excision (TME). Pathological evaluations performed after CRT have demonstrated not only a complete response in some patients but also downstaging of tumor stage. Clinical follow-up of patients who achieved a complete response revealed that their 5 year recurrence and metastasis rates were approximately three times lower than those with a partial response (7-9).

Assessment following nCRT is critical for determining subsequent treatment strategies and predicting the disease course. Although conventional MRI plays a central role in evaluating the extent of disease prior to treatment, it has certain limitations in the post-CRT setting, particularly in distinguishing the primary tumor from radiation-induced fibrosis. MRI assessment in this context is most performed using T2 weighted sequences and apparent diffusion coefficient (ADC) maps derived from diffusion-weighted imaging (DWI) (10). Texture analysis is fundamentally based on computer-assisted data processing, in which statistical parameters are derived from imaging datasets. In recent years, it has been increasingly applied across a broad range of clinical domains, particularly in the field of oncological imaging. In digital images, each pixel and voxel is represented by a specific gray-level intensity value. Quantitative statistical features can be extracted by evaluating the distribution and interrelationships of these gray levels using various mathematical approaches. These parameters provide objective information that facilitates the interpretation of digital medical images and contributes to a more comprehensive image analysis (11,12).

This study aimed to employ texture analysis as a novel imaging method to predict the direction and magnitude of response to nCRT in patients with LARC prior to therapy.

## Methods

Ethical approval was obtained from, University of Health Sciences Türkiye, Haydarpaşa Numune Training and Research Hospital on September 11, 2023 (decision number: HNEAH-KAEK 2023/163, HNEAH-KAEK 2023/KK/163). Given the retrospective design of the study, the requirement to obtain written informed consent from the patients was waived by the committee.

### Study Population

Patients diagnosed with LARC between 2018 and 2025 were retrospectively reviewed using Haydarpaşa Numune Training and Research Hospital institutional Picture Archiving and Communication System (PACS) database. Individuals with locally advanced disease who received nCRT were eligible for inclusion. Patients with a histopathological diagnosis of mucinous adenocarcinoma, patients without available pathological confirmation, and patients who had undergone surgery at an external institution were excluded from the analyses. Haydarpaşa Numune Training and Research Hospital is equipped with two different MRI scanners; for the purposes of this study, only the cohort imaged with the scanner that contributed to the greater number of examinations was evaluated. Patients imaged with heterogeneous or non-standard MRI sequences were excluded. Ultimately, 47 patients who fulfilled the inclusion criteria were enrolled in this study.

In summary, patients meeting any of the following criteria were excluded from the study:

- Histopathological diagnosis of mucinous adenocarcinoma
- Imaging performed with a non-standard MRI protocol
- Receipt of neoadjuvant therapy at an external institution
- Surgical resection performed at an external institution
- Inability to tolerate or complete the planned nCRT regimen
- Insufficient image quality for appropriate diagnostic evaluation

### Image Acquisition

MRI was performed using a 1.5-T scanner (General Electric, Milwaukee, WI, USA) with a standard imaging protocol. Following completion of nCRT, post-treatment MRI examinations were performed within 6-8 weeks prior to surgical resection. The protocol included a T2-weighted fast spin-echo sequence [repetition time/echo time (TR/TE), 4556/100 ms; field of view (FOV), 380 × 380 mm; matrix, 224 × 192; slice thickness, 3 mm], an axial DWI sequence (b values, 0, 400, and 800 s/mm$^2$; TR/TE, 2500/65 ms; FOV, 380 × 380 mm; matrix, 224 × 192; slice thickness, 6 mm), and axial T1-weighted images (TR/TE, 4.4/2.1 ms; FOV, 380 × 380 mm; matrix, 300 × 192; slice thickness, 1 mm). Quantitative ADC maps were generated using a monoexponential decay model applied to three b values. Images were obtained in planes oriented perpendicular and parallel to the long axis of the rectal tumor.

### Histopathological Examination

The pathological response (pCR) was assessed in the resection specimens by a pathologist (15 years experience) with extensive expertise in gastrointestinal pathology, ensuring a high level of diagnostic accuracy and consistency. Following detailed histopathological examination, the collected data were systematically categorized according to the pathological TNM classification system, which provides a standardized framework for tumor staging. Furthermore, the degree of response to neoadjuvant treatment was evaluated using the tumor regression grading system proposed by Ryan et al. (13).

### Neoadjuvant Chemoradiotherapy Scheme

All patients received preoperative concurrent CRT. The treatment regimen consisted of a total radiotherapy dose of approximately 52 Gy delivered over a 5-week period, administered five days per week, with an additional boost as indicated. Chemotherapy was administered concurrently either as 5-fluorouracil (425 mg/m$^2$/day) administered during the 1$^{st}$ and 5$^{th}$ weeks of radiotherapy or as capecitabine (825 mg/m$^2$/day) administered 5 days per week throughout the 5-week course of radiotherapy. Surgical resection was performed 6-8 weeks after CRT completion.

### Analysis of Images

Magnetic resonance images, including axial T2 weighted, ADC, and axial contrast enhanced T1 weighted sequences, were exported in Digital Imaging and Communications in Medicine (DICOM) 3.0 format to the Windows 10 operating system (Microsoft Corporation, Seattle, WA, USA), with each sequence processed separately. Image analysis was

performed using the ROIEX 3.1 software. A circular ROI was manually drawn on the slice where the tumor was most clearly visualized, covering approximately two-thirds of the lesion to minimize the inclusion of artifacts. Imaging data were retrieved from the PACS in DICOM format and transferred to a Windows 10 workstation (Microsoft Corporation, Seattle, WA, USA) for subsequent analysis. All eligible images were processed using a custom in-house analysis pipeline developed in MATLAB (R2023b; MathWorks, Natick, MA, USA) (Figure 1).

### Statistical Analysis

The data obtained in this study are presented as mean ± standard deviation (SD). Statistical analyses were conducted using IBM SPSS for Windows version 26.0 (IBM Statistics, IBM Corporation, Armonk, NY, USA). The Kolmogorov-Smirnov and chi-square tests were applied to assess the normality of the data distribution. Depending on the results, group comparisons were performed using the Mann-Whitney U test. For parameters showing statistical significance ($p<0.05$), receiver operating characteristic (ROC) curve analysis was conducted to determine the sensitivity and specificity. Logistic regression analysis was performed to further assess the predictive value of significant parameters.

To evaluate the treatment response in a standardized and reproducible manner, patients were stratified into two distinct groups according to the tumor regression grading system proposed by Ryan et al. (13). Specifically, patients classified as grade 0 (no viable cancer cells) or grade 1 (single cells or small groups of cancer cells) were assigned to the first group, which was defined as a favorable response to neoadjuvant therapy. In contrast, patients graded as 2 (residual cancer with evident tumor regression but more than single cells or rare groups of cancer cells) or grade 3 (extensive residual cancer with no evidence of regression) were assigned to the second group, which was considered to reflect a poor or unfavorable response to neoadjuvant chemotherapy. This dichotomization allowed for a clear comparison between patients demonstrating effective tumor regression and those exhibiting limited or absent responses to treatment.

## Results

A total of 47 patients diagnosed with LARC were enrolled in this study. Upon evaluation of the collected data, 28 and 19 patients were identified as male and female, respectively, and no statistically significant difference in treatment response was detected between the two sexes.

Texture analysis was conducted on magnetic resonance images obtained from three distinct sequences: T2-weighted imaging, ADC maps, and contrast-enhanced T1-weighted imaging.

In the T2 weighted sequence, the parameters mean, root mean square, root sum of squares, 10$^{th}$ percentile, 25$^{th}$ percentile, 90$^{th}$ percentile, 95$^{th}$ percentile, 97$^{th}$ percentile, entropy, and contrast of matrix were significantly lower in the treatment-responsive group. In contrast, the energy of matrix, homogeneity of matrix and Higuchi Fractal dimension of matrix were significantly higher among responders (Table 1).

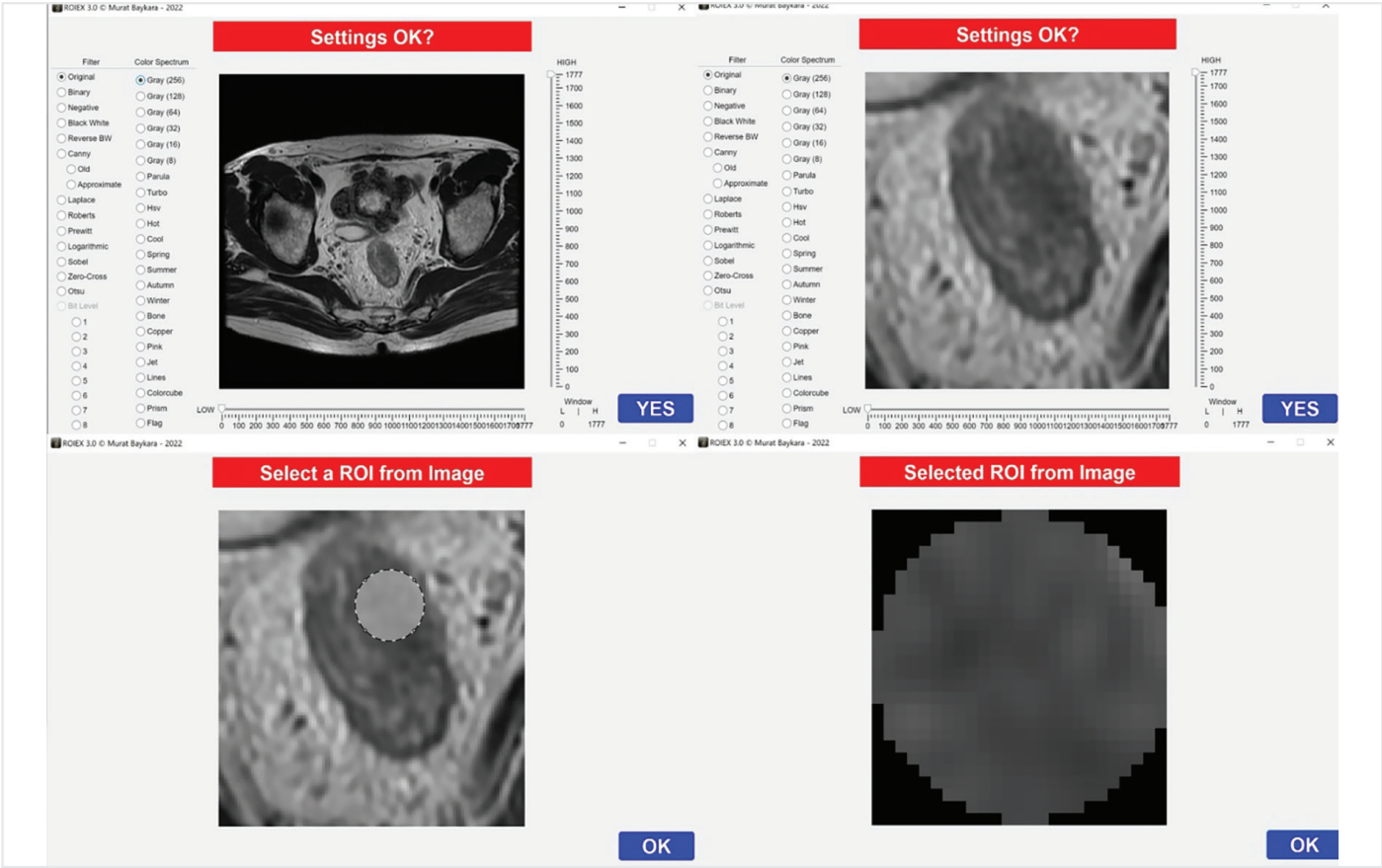


**Figure 1.** ROI selection steps on the DICOM image from the slice in which the tumor is most clearly visualized. ROI: Region of interest, DICOM: Digital Imaging and Communications in Medicine

**Table 1. Parameters showing a statistically significant difference**

| Group statistics | No response | (27) | Response | (20) | p values |
|---|---|---|---|---|---|
| | Mean | SD | Mean | SD | |
| T2-mean of histogram | 381.1469 | 69.3931 | 340.3331 | 76.6852 | 0.037 |
| T2-root-mean-square level of histogram | 383.6346 | 69.2325 | 342.8661 | 76.8468 | 0.039 |
| T2-root-sum-of-squares level of histogram | 5762.7972 | 2577.1566 | 3684.8846 | 1370.2391 | 0.001 |
| T2-10$^{th}$ percentile of histogram | 330.4222 | 69.4563 | 288.4700 | 72.1472 | 0.034 |
| T2-25$^{th}$ percentile of histogram | 354.3889 | 70.0191 | 311.9625 | 73.6861 | 0.031 |
| T2-90$^{th}$ percentile of histogram | 434.5407 | 74.1257 | 392.5950 | 88.6851 | 0.037 |
| T2-95$^{th}$ percentile of histogram | 453.8889 | 78.6010 | 410.3600 | 92.6228 | 0.032 |
| T2-97$^{th}$ percentile of histogram | 465.5100 | 83.5031 | 421.3390 | 95.9464 | 0.045 |
| T2-entropy of histogram | 6.3832 | 0.5270 | 5.9762 | 0.4984 | 0.011 |
| T2-contrast of matrix | 41.7244 | 33.7833 | 20.2681 | 10.5748 | 0.001 |
| T2-energy of matrix | 0.0060 | 0.0036 | 0.0108 | 0.0056 | 0.001 |
| T2-homogeneity of matrix | 0.2591 | 0.0566 | 0.3051 | 0.0438 | 0.009 |
| T2-Higuchi fractal dimension of matrix | 1.4483 | 0.0822 | 1.5209 | 0.1391 | 0.045 |
| ADC-minimum of histogram | 739.0769 | 211.0175 | 906.0500 | 213.6523 | 0.010 |
| ADC-1$^{st}$ percentile of histogram | 743.4665 | 209.5699 | 910.4635 | 211.8027 | 0.011 |
| ADC-3$^{rd}$ percentile of histogram | 774.8658 | 208.4411 | 934.6525 | 205.2943 | 0.012 |
| ADC-5$^{th}$ percentile of histogram | 796.7981 | 212.2147 | 960.6175 | 209.5846 | 0.012 |
| ADC-10$^{th}$ percentile of histogram | 840.9000 | 217.7492 | 1008.3700 | 225.2577 | 0.015 |
| ADC-25$^{th}$ percentile of histogram | 926.9615 | 231.0978 | 1096.8500 | 241.7372 | 0.022 |
| ADC-entropy of histogram | 5.7332 | 0.4331 | 5.1167 | 0.5817 | <0.001 |
| ADC-entropy of matrix | 5.0015 | 0.3554 | 4.6278 | 0.5114 | 0.007 |
| ADC-uniformity of matrix | 0.4067 | 0.1078 | 0.4694 | 0.0897 | 0.028 |
| ADC-mean local entropy of matrix | 4.4500 | 0.2090 | 4.2794 | 0.3330 | 0.049 |
| ADC-contrast of matrix | 13.4676 | 5.9924 | 8.2755 | 5.3938 | <0.001 |
| ADC-energy of matrix | 0.0163 | 0.0060 | 0.0277 | 0.0111 | <0.001 |
| ADC-homogeneity of matrix | 0.3393 | 0.0535 | 0.4053 | 0.0542 | <0.001 |
| ADC-low gray-level zone emphasis of GLSZM | 0.1150 | 0.0586 | 0.0845 | 0.0431 | 0.039 |
| ADC-absolute gradient skewness of histogram-"Sobel" | 1.2490 | 0.5924 | 0.9503 | 0.3893 | 0.049 |
| ADC-absolute gradient skewness of histogram-"Prewitt" | 1.2490 | 0.5924 | 0.9503 | 0.3893 | 0.049 |
| ADC-absolute gradient skewness of matrix-"Sobel" | 0.1927 | 0.3552 | -0.1374 | 0.3784 | 0.012 |
| ADC-absolute gradient skewness of matrix-"Prewitt" | 0.1991 | 0.3417 | -0.1205 | 0.3646 | 0.007 |
| ADC-absolute gradient skewness of matrix-"Central" | 0.1696 | 0.5578 | -0.2682 | 0.5758 | 0.016 |
| ADC-AR model - initial states of state-space realization | 879.7952 | 381.8013 | 630.8040 | 344.1450 | 0.020 |
| T1+C-mean of histogram | 858.0034 | 297.4355 | 957.8116 | 173.7738 | 0.045 |
| T1+C-root-mean-square level of histogram | 862.5253 | 297.2398 | 963.0566 | 175.4708 | 0.048 |
| T1+C-25$^{th}$ percentile of histogram | 802.3889 | 292.4160 | 897.9875 | 166.2323 | 0.047 |
| T1+C-75$^{th}$ percentile of histogram | 913.2222 | 307.0603 | 1020.0375 | 196.8879 | 0.047 |
| T1+C-entropy of histogram | 6.5048 | 0.5482 | 6.2189 | 0.3923 | 0.023 |
| T1+C-mean local range of matrix | 381.0235 | 15.5574 | 471.3626 | 87.6760 | 0.007 |
| T1+C-mean local standard deviation of matrix | 153.5272 | 64.3133 | 191.2951 | 34.6884 | 0.006 |
| T1+C-contrast of matrix | 33.4492 | 18.1704 | 21.0826 | 8.6546 | 0.013 |
| T1+C-energy of matrix | 0.0072 | 0.0052 | 0.0096 | 0.0044 | 0.016 |
| T1+C-homogeneity of matrix | 0.2715 | 0.0557 | 0.3032 | 0.0458 | 0.037 |
| T1+C-AR model - estimated "A" polynomial parameters | -0.9947 | 0.0106 | -0.9925 | 0.0102 | 0.037 |

SD: Standard deviation, ADC: Apparent diffusion coefficient, GLSZM: Gray level size zone matrix

In the ADC sequence, the following features were significantly lower in the treatment-responsive group: entropy of histogram; entropy of matrix; mean local entropy of matrix; contrast of matrix; low gray-level zone emphasis of gray level size zone matrix; absolute gradient skewness of histogram; absolute gradient skewness of matrix-"Sobel"; absolute gradient skewness of matrix-"Prewitt"; ADC-absolute gradient skewness of matrix-"Central"; and ADC-AR model-initial states of state-space realization. Conversely, the minimum of histogram, 1st, 3rd, 5th, 10th, and 25th percentiles, uniformity of matrix, energy of matrix, and homogeneity of matrix were significantly higher in the responder group (Table 1).

In the contrast enhanced T1 weighted sequence, the Entropy of Histogram and Contrast of Matrix were significantly lower in patients who responded to therapy. Meanwhile, the mean of histogram, root mean square level, 25th percentile of histogram, 75th percentile of the histogram, mean local range of the matrix, mean local SD of the matrix, energy of the matrix, homogeneity of the matrix, and AR model-estimated "A" polynomial were significantly higher in the treatment-responsive group (Table 1).

For all other assessed texture parameters, no statistically significant differences were identified between the treatment-responsive and non-responsive groups.

ROC analyses were performed for several parameters that exhibited strong statistical significance, and the corresponding area under the curve, sensitivity, and specificity values obtained at the optimal cut-off thresholds for discriminating between the two groups are summarized in (Figures 2-4).

The logistic regression analysis was statistically significant [$\chi^2$ (9): 37.183, $p<0.001$]. The ENTER model accounted for 74.3% of the variance in treatment response, as indicated by the Nagelkerke $R^2$ value, and correctly classified 91.3% of patients with respect to their response to the therapy. These findings demonstrate that the model possesses substantial explanatory power and a high level of predictive accuracy, supporting its utility in identifying individuals who are likely to respond to the treatment. In the constructed model, an increase in the contrast of matrix parameter within the ADC sequence and decreases in the contrast of matrix and energy of matrix parameters within the contrast-enhanced T1- weighted sequence were identified as significant contributors to the model's predictive capacity. These texture features demonstrated meaningful associations with the treatment response and played an important role in enhancing the discriminative performance of the model.

## Discussion

In this study, we aimed to predict the therapeutic response in patients with LARC who underwent nCRT by performing a comprehensive texture analysis of pretreatment MRI scans. The overarching objective was to determine whether quantitative imaging biomarkers derived from baseline MRI could reliably characterize tumor heterogeneity and serve

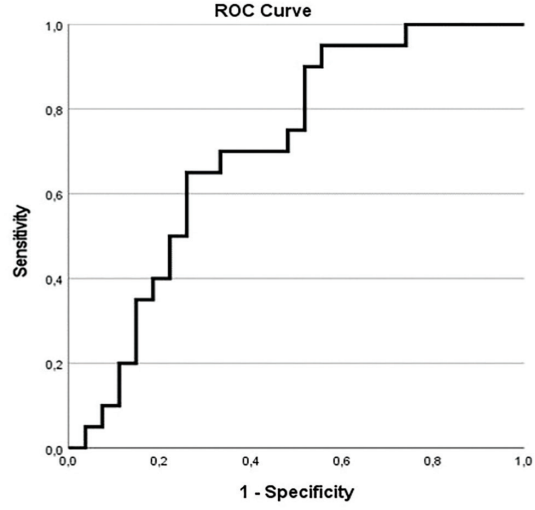


**Figure 3.** Receiver operating characteristic (ROC) curve for the contrast-enhanced T1 energy of the matrix parameter

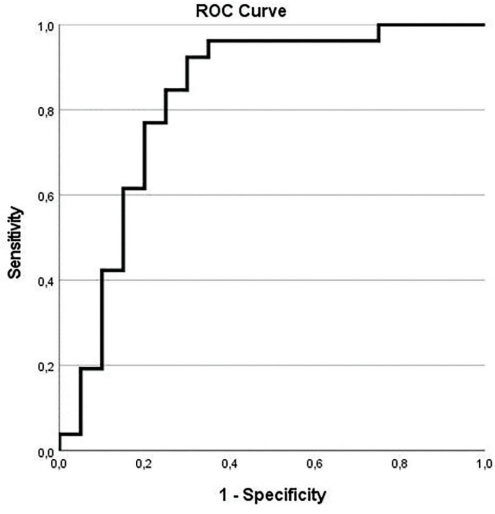


**Figure 2.** Receiver operating characteristic (ROC) curve for the apparent diffusion coefficient contrast of the matrix parameter

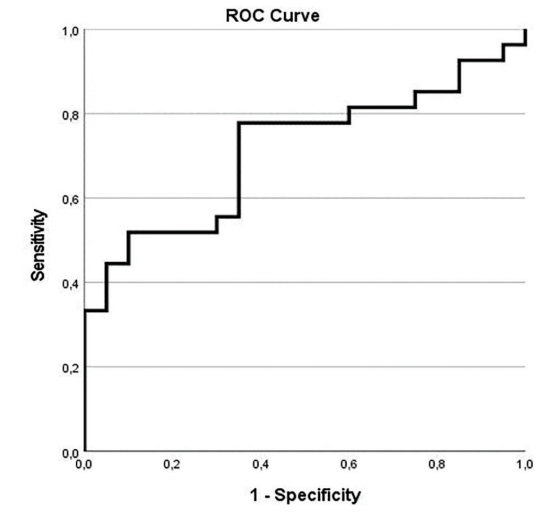


**Figure 4.** Receiver operating characteristic (ROC) curve for the contrast-enhanced T1 contrast of the matrix parameter

as predictors of subsequent treatment response. This approach aims to contribute to the development of precision medicine strategies that enable individualized treatment planning and improved clinical outcomes for patients with LARC.

For treatment response assessment, pre-treatment MRI images were analyzed using texture analysis across three different sequences, with 277 texture features being extracted from each sequence. Among all evaluated features, 44 parameters demonstrated statistically significant differences between the response groups. In the multivariate analysis, three parameters emerged as independent predictors of therapeutic response (Table 2).

In current oncological practice, the standard treatment approach for LARC consists of nCRT, followed by TME. This combined strategy aims to reduce the tumor burden, facilitate surgical resection, and minimize the risk of local recurrence (8). Pathological assessment after CRT isthe most reliable method for determining the extent of therapeutic response. In a subset of patients, this evaluation revealed a complete pCR or tumor downstaging, reflecting a significant reduction or even disappearance of viable tumor cells. These findings not only demonstrate the biological effectiveness of CRT but also highlight the heterogeneity of individual treatment responses among patients with rectal cancer. Moreover, numerous studies have shown that patients who achieve a pCR exhibit markedly improved clinical outcomes, including lower rates of local recurrence and distant metastasis, as well as higher overall survival rates,compared to those with partial or poor response. These observations underscore the prognostic value of treatment response following nCRT (9,10).

In recent years, numerous studies have focused on tissue evaluation using texture analysis, and its clinical adoption has steadily increased, reflecting its growing value as a quantitative imaging biomarker (14,15). The utility of this methodology extends across a wide clinical continuum, encompassing conditions from neurological spectrum disorders to complex oncological processes. This breadth of application underscores its ability to quantify subtle tissue alterations across diverse pathologies, thereby contributing to more precise diagnostic assessment, refined disease stratification, and optimized therapeutic decision-making (16,17).

Malignant tumors inherently exhibit intratumoral heterogeneity owing to their intrinsic biological structures. As a result of this heterogeneity, tumors may vary considerably in both prognosis and response to administered treatments. Texture analysis allows the quantitative evaluation of these heterogeneous intratumoral patterns and may enable the early identification of potential resistance to nCRT (18,19).

In contrast enhanced T1weighted sequences, the energy of matrix value was higher in the responder group, and a decrease in this value strengthened the prediction of treatment response. Similarly, Meng et al. (20) reported in their study that energy values were higher among patients responding to treatment. Our findings indicate that T2 weighted histogram entropy did not independently predict treatment response, yet responders exhibited lower values, corroborating another study (21). The minimum histogram value on the ADC sequence differed between responders and non-responders, consistent with the findings of a previous study (22). In another previous study (23), the minimum ADC histogram values at the $10^{th}$ and $25^{th}$ percentiles differed significantly according to treatment response. Similarly, in our cohort, we observed significant differences in these parameters between responders and non-responders. Moreover, we found that the $10^{th}$ and $25^{th}$ percentile values also differed significantly in the T2-weighted sequence, which may further underscore the potential relevance of T2-weighted imaging in response assessment. In contrast, the skewness and kurtosis derived from the ADC did not differ significantly between the two groups (24).

Based on the findings of the present study, the predictive model we developed demonstrated a robust capacity to discriminate between responders and non-responders prior to the initiation of therapy. By integrating key radiomic features with clinically relevant parameters, the model achieved a high level of accuracy, indicating that subtle textural and structural characteristics captured on pretreatment imaging harbor meaningful information regarding tumor biology and treatment susceptibility of the tumor. These results highlight the value of advanced image-based analytics in characterizing intratumoral heterogeneity and underscore the feasibility of using such quantitative metrics for individualized treatment planning. Importantly, the ability of the model to reliably predict treatment response before therapy initiation has significant clinical implications.

### Study Limitations

The present study had some limitations that warrant consideration. The cohort size was relatively small, whereas radiomics studies typically require larger populations to ensure robust and generalizable results. Additionally, ROI delineation was performed in two dimensions on the para-axial plane, and the inclusion of complementary planes may improve the reliability of the extracted features. Manual segmentation also introduces potential inter-observervariability and may increase measurement errors, particularly among less experienced readers. Future studies should evaluate deep learning–based segmentation frameworks to mitigate these limitations.

## Conclusion

Radiomics and mathematical modeling are attracting increasing attention in the medical community because of theirpotential to support clinicians in several ways. In this context, in patients diagnosed with LARC, early identification based on pre-nCRT imaging of those

**Table 2. Logistic regression analysis findings**

| Parameters | b | SE | Wald | df | Sig. | Exp (B) |
|---|---|---|---|---|---|---|
| ADC-contrast of matrix | 0.708 | 0.322 | 4.846 | 1 | 0.028 | 2.031 |
| T1+C-contrast of matrix | -0.418 | 0.201 | 4.315 | 1 | 0.038 | 0.658 |
| T1+C-energy of matrix | -1121.178 | 470.201 | 5.686 | 1 | 0.017 | 0.011 |

ADC: Apparent diffusion coefficient, SE: Standard error, Sig.: Significance, Exp.: Exponentiated

who are unlikely to benefit from standard protocols may facilitate timely modification of treatment strategies, prevent unnecessary toxicity, and enable a more efficient allocation of healthcare resources. Taken together, these findings suggest that radiomics-based predictive modeling may serve as a non-invasive decision support tool for the personalized management of patients undergoing neoadjuvant therapy. We also believe that studies conducted in larger cohorts may achieve higher accuracy in predicting treatment response.

### Ethics

**Ethics Committee Approval:** Ethical approval was obtained from, University of Health Sciences Türkiye, Haydarpaşa Numune Training and Research Hospital on September 11, 2023 (decision number: HNEAH-KAEK 2023/163, HNEAH-KAEK 2023/KK/163).

**Informed Consent:** Given the retrospective design of the study, the requirement to obtain written informed consent from the patients was waived by the committee.

### Footnotes

**Authorship Contributions:** Concept - M.Ö., K.C., E.B., M.B.; Design - M.Ö., K.C., M.B.; Data Collection or Processing - M.Ö., K.C., E.B.; Analysis or Interpretation - M.Ö., K.C., M.B.; Literature Search - M.Ö., K.C., E.B.; Writing - M.Ö., K.C.

**Conflict of Interest:** No conflict of interest was declared by the authors.

**Financial Disclosure:** The authors declared that this study received no financial support.

## References

1. Siegel RL, Miller KD, Goding Sauer A, Fedewa SA, Butterly LF, Anderson JC, et al. Colorectal cancer statistics, 2020. CA Cancer J Clin. 2020; 70: 145-64.
2. Ferlay J, Colombet M, Soerjomataram I, Dyba T, Randi G, Bettio M, et al. Cancer incidence and mortality patterns in Europe: Estimates for 40 countries and 25 major cancers in 2018. Eur J Cancer. 2018; 103: 356-87.
3. Horvat N, Carlos Tavares Rocha C, Clemente Oliveira B, Petkovska I, Gollub MJ. MRI of rectal cancer: tumor staging, imaging techniques, and management. Radiographics. 2019; 39: 367-87.
4. Siddiqui MRS, Simillis C, Hunter C, Chand M, Bhoday J, Garant A, et al. A meta-analysis comparing the risk of metastases in patients with rectal cancer and MRI-detected extramural vascular invasion (mrEMVI) vs mrEMVI-negative cases. Br J Cancer. 2017; 116: 1513-9.
5. Lord AC, D'Souza N, Pucher PH, Moran BJ, Abulafi AM, Wotherspoon A, et al. Significance of extranodal tumour deposits in colorectal cancer: a systematic review and meta-analysis. Eur J Cancer. 2017; 82: 92-102.
6. Al-Sukhni E, Milot L, Fruitman M, Beyene J, Victor JC, Schmocker S, et al. Diagnostic accuracy of MRI for assessment of T category, lymph node metastases, and circumferential resection margin involvement in patients with rectal cancer: a systematic review and meta-analysis. Ann Surg Oncol. 2012; 19: 2212-23.
7. Sauer R, Becker H, Hohenberger W, Rödel C, Wittekind C, Fietkau R, et al. Preoperative versus postoperative chemoradiotherapy for rectal cancer. N Engl J Med. 2004; 351:1731-40.
8. Glimelius B, Tiret E, Cervantes A, Arnold D; ESMO Guidelines Working Group. Rectal cancer: ESMO Clinical Practice Guidelines for diagnosis, treatment and follow-up. Ann Oncol. 2013; 24 Suppl 6: vi81-8.
9. Martin ST, Heneghan HM, Winter DC. Systematic review and meta-analysis of outcomes following pathological complete response to neoadjuvant chemoradiotherapy for rectal cancer. Br J Surg. 2012; 99: 918-28.
10. Kim SH, Lee JM, Hong SH, Kim GH, Lee JY, Han JK, et al. Locally advanced rectal cancer: added value of diffusion-weighted MR imaging in the evaluation of tumor response to neoadjuvant chemo- and radiation therapy. Radiology. 2009; 253: 116-25.
11. Scapicchio C, Gabelloni M, Barucci A, Cioni D, Saba L, Neri E. A deep look into radiomics. Radiol Med. 2021; 126: 1296-311.
12. Castellano G, Bonilha L, Li LM, Cendes F. Texture analysis of medical images. Clin Radiol. 2004; 59: 1061-9.
13. Ryan R, Gibbons D, Hyland JM, Treanor D, White A, Mulcahy HE, et al. Pathological response following long-course neoadjuvant chemoradiotherapy for locally advanced rectal cancer. Histopathology. 2005; 47: 141-6.
14. Baykara M, Baykara S. Texture analysis of dorsal striatum in functional neurological (conversion) disorder. Brain Imaging Behav. 2022; 16: 596-607.
15. Baykara M, Yildirim M. Differentiation of multiple myeloma and metastases with apparent diffusion coefficient map histogram analysis. North Clin Istanb. 2022; 9: 256-60.
16. Baykara M, Baykara S. Is the caudate, putamen, and globus pallidus the delusional disorder's trio? A texture analysis study. Actas Esp Psiquiatr. 2024; 52: 256-67.
17. Azamat S, Karaman Ş, Azamat IF, Ertaş G, Kulle CB, Keskin M, et al. Complete response evaluation of locally advanced rectal cancer to neoadjuvant chemoradiotherapy using textural features obtained from T2 weighted imaging and ADC maps. Curr Med Imaging. 2022; 18: 1061-9.
18. Fu F, Nowak MA, Bonhoeffer S. Spatial heterogeneity in drug concentrations can facilitate the emergence of resistance to cancer therapy. PLoS Comput Biol. 2015; 11: e1004142.
19. Hardiman KM, Ulintz PJ, Kuick RD, Hovelson DH, Gates CM, Bhasi A, et al. Intra-tumor genetic heterogeneity in rectal cancer. Lab Invest. 2016; 96: 4-15.
20. Meng Y, Zhang C, Zou S, Zhao X, Xu K, Zhang H, et al. MRI texture analysis in predicting treatment response to neoadjuvant chemoradiotherapy in rectal cancer. Oncotarget. 2017; 9: 11999-2008.
21. Staal FCR, van der Reijd DJ, Taghavi M, Lambregts DMJ, Beets-Tan RGH, Maas M. Radiomics for the prediction of treatment outcome and survival in patients with colorectal cancer: a systematic review. Clin Colorectal Cancer. 2021; 20: 52-71.
22. Cantürk A, Yarol RC, Tasak AS, Gülmez H, Kadirli K, Bişgin T, et al. Comparative analysis of tumor and mesorectum radiomics in predicting neoadjuvant chemoradiotherapy response in locally advanced rectal cancer. Diagn Interv Radiol. 2026; 32: 365-75.
23. Choi MH, Oh SN, Rha SE, Choi JI, Lee SH, Jang HS, et al. Diffusion-weighted imaging: apparent diffusion coefficient histogram analysis for detecting pathologic complete response to chemoradiotherapy in locally advanced rectal cancer. J Magn Reson Imaging. 2016; 44: 212-20.
24. Enkhbaatar NE, Inoue S, Yamamuro H, Kawada S, Miyaoka M, Nakamura N, et al. MR imaging with apparent diffusion coefficient histogram analysis: evaluation of locally advanced rectal cancer after chemotherapy and radiation therapy. Radiology. 2018; 288: 129-37.